Safer and stronger together? Effects of the agglomeration on nanopowders explosion

Audrey Santandrea, Stéphanie Pacault, Sébastien Bau, Yohan Oudart, Alexis Vignes, Laurent Perrin, Olivier Dufaud

Safer and stronger together? Effects of the agglomeration on nanopowders explosion

Audrey Santandrea [1,2], Stéphanie Pacault [1], Sébastien Bau [3], Yohan Oudart [4], Alexis Vignes [2], Laurent Perrin [1], Olivier Dufaud [1,*]

***Corresponding author:** Olivier Dufaud (E-mail address: olivier.dufaud@univ-lorraine.fr)

[1] Université de Lorraine, CNRS, LRGP, F-54000 Nancy, France

[2] INERIS, Accidental Risks Division, Parc Technologique ALATA, BP 2, F-60550, Verneuil-en-Halatte, France

[3] INRS, 1 rue du Morvan CS 60027, 54519, Vandoeuvre-lès-Nancy, France

[4] Nanomakers, 1 rue de Clairefontaine, 78120 Rambouillet, France

Abstract:

Among the factors influencing dust explosion, the particle size distribution (PSD) is both one of the most important and complex to consider. For instance, it is commonly accepted that the explosion sensitivity increases when the particle size decreases. Such an assertion may be questionable for nano-objects which easily agglomerate. However, agglomerates can be broken during the dispersion process. Correlating the explosion parameters to the actual PSD of a dust cloud at the moment of the ignition becomes then essential. The effects of the moisture content and sieving were investigated on a nanocellulose powder and the impact of a mechanical agglomeration was evaluated using a silicon coated by carbon powder. Each sample was characterized before and after dispersion using in situ laser particle size measurement and a fast mobility particle sizer, and explosion and minimum ignition energy

tests were conducted respectively in a 20 L sphere and in a modified Hartmann tube. It was observed that drying and/or sieving the nanocellulose mainly led to variations in terms of ignition sensitivity but only slightly modified the explosion severity. In contrast, the mechanical agglomeration of the silicon coated by carbon led to a great decrease in terms of ignition sensitivity, with a minimum ignition energy varying from 5 mJ for the raw powder to more than 1J for the agglomerated samples. The maximum rate of pressure rise also decreased due to modifications in the reaction kinetics, inducing a transition from St2 class to St1 class when agglomerating the dust.

Keywords: Dust explosion; Nanoparticles; Agglomeration; Dispersion

1. Introduction

According to the European Commission (2011/696/EU, 2011), a nanomaterial is "a natural, incidental or manufactured material containing particles, in an unbound state or as an aggregate or as an agglomerate and where, for 50% or more of the particles in the number size distribution, one or more external dimensions is in the size range 1 nm – 100 nm". This recommendation also specifies that any material presenting a specific surface area by volume of the material higher than 60 $m^2.cm^{-3}$ must be considered as a nanomaterial. This small size induces additional, enhanced or different properties for the nanomaterials, which implies that the fundamental properties such as chemical, mechanical, optical or biological properties are modified and often innovative (Stark et al., 2015). Those new properties resulted to an increasing interest in nanoparticles for applications in different fields, like health, automotive industry, construction, food or electronic sector, but also generated a question concerning the

toxicity of the materials (Oberdörster et al., 2005). But nanoparticles, as well as any combustible particles, present another important risk: their dispersion under certain conditions and in the presence of an ignition source can lead to an explosion.

If dust explosion risks concerning micron-sized particles can be relatively well estimated, it is not yet the case for nanoparticles. Indeed, the interest in nanotechnologies and in their specific properties is quite recent and there are only a few feedbacks on accidental dust explosions involving nanoparticles (Wu et al., 2014). Some laboratory tests were already carried out to evaluate the ignition sensitivity and explosivity of nanopowders (Boilard et al., 2013; Holbrow et al., 2010; Krietsch et al., 2015; Wu et al., 2009). It appears that powders are usually more sensitive to ignition, but no significant variation concerning the explosion severity was observed (Bouillard et al., 2010; Dufaud et al., 2011; Holbrow et al., 2010). This phenomenon is mainly explained by the agglomeration and aggregation phenomenon induced by the small size of the nanoparticles, which reduces the reactive surface area and decreases the explosion severity (Eckhoff, 2011, 2012).

Generally, a nanopowder is comprised of primary nanoparticles, i.e. individual nanoparticles, which aggregate, forming so-called “primary aggregates”, which themselves agglomerate with each other. An agglomerate consists of weakly bonded particles that can be separated while an aggregate is an assembly of strongly bonded particles that cannot be broken (Sokolov et al., 2015; Walter, 2013). The main cohesion forces inducing the agglomeration of nanoparticles aggregates are the van der Waals interactions, electrostatic and magnetic forces, and, in the case of wet particles, capillary effects (Debrincat et al., 2008; Hartley et al., 1985). Each agglomerate then possesses a cohesion strength that can be calculated by different ways (Kendall, 1988; Rumpf, 1962; Weiler et al., 2010). In order to break an agglomerate, an energy higher than the cohesion strength must be provided, leading back to the primary aggregates.

For an explosion to occur, some conditions are needed. Among them is the dispersion of the powder, which can break the agglomerates, at least partially, depending on the shear stress occurring during the dust dispersion. Since the particle size distribution (PSD) is a very important parameter influencing dust explosion, it becomes necessary to characterize the dust cloud not only before its dispersion, but also at the exact ignition time (Santandrea et al., 2019b). Moreover, it is imperative to choose wisely the operating conditions for the explosion tests, to be sure to evaluate the worst -but realistic- case scenario. Indeed, the standard conditions were established for micron-sized particles and are currently applied when testing nanoparticles. However, these conditions may need to be adapted due to the specific properties of nanomaterials (Santandrea et al., 2020).

The impact of the agglomeration on the explosion severity of nanopowders was evaluated by modifying the agglomerates size and cohesion strength before their dispersion and performing explosion tests in a 20 L sphere according to international standards (EN 14034-1, 2004; EN 14034-2, 2006). Since the addition of a cohesive agent would modify the reactions involved in the explosion, three main ways can be considered: grinding, selection (sieving), and mechanical agglomeration (e.g. wet or dry granulation, compaction). The dispersion procedure in the 20 L sphere already inducing a high shear stress due to the pressurization of the dust container at 20 barg, it would be difficult to further reduce the size of the agglomerates after dispersion. Indeed, the smaller the particle (or agglomerate), the harder it is to be broken (Deng et al., 2016). Moreover, dry powder grinding would not allow to obtain agglomerates smaller than around 1 µm, and the process would produce heat and possibly electrostatic discharges that could be sufficient to ignite the most sensitive powders. Therefore, powder grinding was not considered as a suitable solution. The effects of the agglomeration on the explosion severity and ignition sensitivity were then investigated by

sieving and by mechanical agglomeration, respectively on nanocellulose and carbon coated silicon powders.

2. Materials and methods

2.1. Materials

The effects of nanopowders agglomeration on their explosivity were investigated using two different materials. First, a nanocrystalline cellulose (NCC from CelluForce), called 'nanocellulose', was chosen due to its organic nature and wide range of applications. This powder is constituted of primary nanofibers of 3 nm width and an average length of 70 nm which form agglomerates with diameters ranging between 1 µm and several dozens of micrometers, as presented in Figure 1. To avoid the influence of humidity on both agglomeration state (capillary effects) and explosion characteristics, which was discussed by Santandrea et al. (2020), this powder was systematically dried at 90°C under vacuum. The water activity, i.e. the partial vapor pressure of water divided by the standard state partial vapor pressure of water, was measured around 0.03 after drying (Aw-meter, Rotronic), confirming that no additional water present in the powder would participate to the combustion. In an attempt to obtain different agglomerate sizes, the nanocellulose was sieved using a 40 µm mesh strainer submitted to low amplitude vibrations to avoid the breakage of the agglomerates. This procedure then allows the separation of the biggest agglomerates from the finest particles.

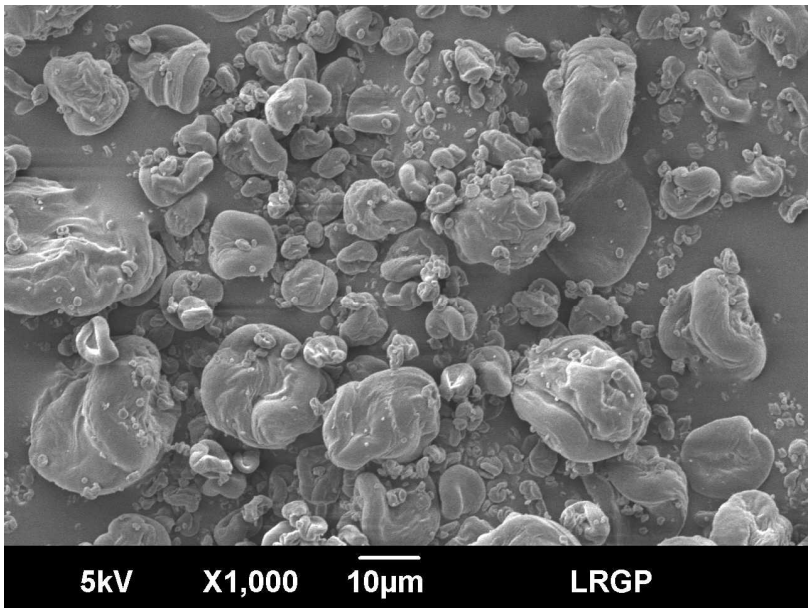

Figure 1. Raw nanocellulose observed by Scanning Electron Microscopy

Complementary to the PSD selection performed on nanocellulose, the effects of a mechanical agglomeration without any additive were investigated on carbon coated silicon, noted 'SiΩC', through different agglomerated samples directly supplied by Nanomakers. Due to the low density of the nanoparticles, such modification notably facilitates the transportation of the powder and increases the powder flowability. Contrary to the nanocellulose, the powder was not dried to avoid the breakage of the agglomerates, as the mechanical agglomeration was realized directly on the raw powder without any additive. Moreover, the oxidation of silicon in the presence of water can lead to the formation of hydrogen (Mehta et al., 2014), which would increase the explosion severity. In this case, drying the powder would probably lead to an underestimation of the safety parameters of the powders.

Four samples of carbon coated silicon constituted of the same powder with different densities, agglomerates sizes and cohesion strengths were then studied in this work: the raw powder of primary diameter of 40 nm and density of 40 $g.L^{-1}$, two samples agglomerated according to a process noted 'process A' with bulk densities of respectively 260 $g.L^{-1}$ and 400 $g.L^{-1}$, which will be noted powders A1 and A2, and a sample agglomerated according to a 'process B' with

131 a bulk density of 400 g.L^{-1}, noted sample B. The specific processes of agglomeration are
132 confidential and unfortunately cannot be described here. Scanning Electron Microscopy
133 analyses were performed on each sample, without any modification, to visualize the shape
134 modifications due to the agglomeration (Figure 2).

135 The raw powder appears to be constituted of small spherical agglomerates of apparent
136 diameters lower than 10 µm, as shown in Figure 2a. The modified powders also present the
137 same kind of agglomerated structures, but also bigger agglomerates. Indeed, the powder A1
138 seems essentially composed of big 'roughly spherical' agglomerates with a diameter around
139 100 to 200 µm (Figure 2b). Similar agglomerates can be found in the sample A2, but with
140 agglomerates size around 300 µm (Figure 2c). Finally, when using the process B to
141 agglomerate the powder, non-spherical agglomerates with an average size reaching 500 µm
142 were formed (Figure 2d).

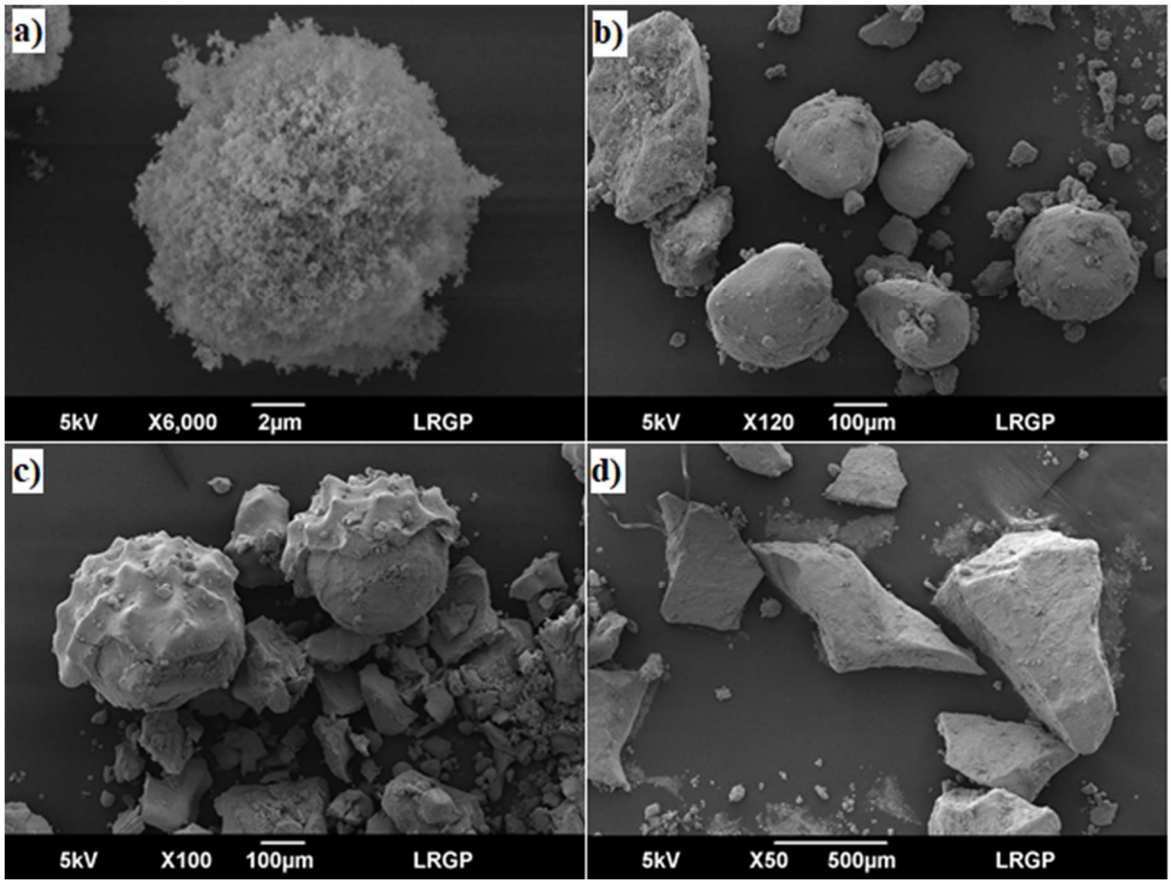

Figure 2. Carbon-coated silicon observed by Scanning Electron Microscopy a) Raw powder b) Sample A1 (260 g.L^{-1}) c) Sample A2 (400 g.L^{-1}) d) Sample B (400 g.L^{-1})

2.2. Methods

The initial particle size distribution (PSD), i.e. before dispersion in the testing equipment, of each sample of nanocellulose and carbon coated silicon was measured in air using a laser diffraction HELOS/KR-Vario (Sympatec GmbH). The PSD was characterized by sedimentation of the powders in the measuring area of the apparatus. As this process was realized manually (by sprinkling powders with a spatula shaken at a constant height), it may therefore be questioned in terms of repeatability. Nevertheless, several tests on each sample led to similar PSD, which then gives a good order of magnitude of the PSD of the dust cloud submitted to very low shear rates. In this study, the surface fraction was considered instead of the 'commonly-used' volume fraction when analyzing the PSD in order to highlight the

surface specificities of nanoparticles. Moreover, when considering the volume fraction, the high volume of big agglomerates tends to occult the presence of smaller nano-agglomerates. Thus, the volume fraction measured by the apparatus was converted into a surface fraction using the equivalent volume diameter.

Since the dispersion procedure, required to produce a dust explosion induces a shear stress that can potentially break the agglomerates, PSD measurements were conducted after dispersion in the explosion vessel. However, no apparatus or technique currently allow the determination of a PSD over a wide range from 10 nm (primary particles) to 500 µm (agglomerates), at high concentration (above the lower explosion limit or at least at a few $g.m^{-3}$) and at high frequency (each millisecond or at least each 10 ms). Thus, different techniques were combined. The dust dispersion was realized in a 20 L sphere equipped with windows according to the same procedure than during explosion tests: the weighed sample is placed in the dust container, and the sphere is evacuated to 0.4 bara. The container is then pressurized 20 barg and the electrovalve connecting the dust canister to the explosion chamber opens, inducing the dispersion of the powder. Contrary to explosion tests, no ignition was performed, and the time evolution of the PSD was recorded.

The laser diffraction sensor (Helos - Sympatec) used to measure the initial PSD of the dust before dispersion was attached to the 20 L sphere equipped with visualization windows made of borosilicate with a diameter of 9.7 cm to allow optical measurements (Murillo, 2016). The PSD was then measured at the place of ignition using various lenses (called R1, R3 and R5) and systematically presented at the moment of ignition, i.e. 60 ms after the beginning of the dispersion according to EN 14034 1&2 (2004; 2006). The boundaries of the measurement ranges are 0.1 – 35 µm, 0.5 – 175 µm and 0.5 – 875 µm for R1, R3 and R5 lenses, respectively. It should be noted that the maximum distance between the lens and the sample is 20 mm for R1, whereas it can reach 47 cm for R5. As a consequence, only the powder located

near the observation windows will be analyzed by using R1, whereas the other lenses will give a PSD representative of the overall content of the sphere.

The presence of nanoparticles after dispersion of nanocellulose and carbon coated silicon in the 20 L sphere was also investigated using a Fast Mobility Particle Sizer (FMPS - TSI) measuring electrical mobility diameters from 5.6 to 560 nm with 1 Hz time resolution and a Scanning Mobility Particle Sizer (SMPS), providing one measurement every two minutes. Despite the low frequency and mass concentration which prevent an accurate characterization, the observation of nanoparticles up to two minutes after dispersion, with particle size distribution ranging from 10 to 400 nm, implies that such particles were also present a few dozens of milliseconds after dispersion.

The explosion severity of each sample was measured in a standard 20 L sphere according to EN 14034 1&2 (2004; 2006), i.e. using two chemical igniters of 5 kJ each and an ignition delay time, tv of 60 ms. The 20 L sphere is equipped with a cooling jacket with water at 300 K. The minimum ignition energy (MIE) of the samples was measured using a standard modified Hartmann tube according to ISO/IEC 80079-20-2 (2016). Although international standards EN 14034-3 (2006) recommend to measure the lower explosion limit in the 20 L sphere using an ignition energy of 2 kJ, this parameter was approximated in the same conditions as the explosion severity tests, i.e. for an ignition energy of 10 kJ.

3. Results and discussions

3.1. Effects of particle size selection: example of nanocellulose

As detailed in section 2.1, the nanocellulose was dried and sieved using a 40 µm mesh strainer. The particle size distribution of each fraction was measured using the laser diffraction sensor (R3 lens) by sedimentation. The upper fraction was constituted of agglomerates of sizes between 40 and 100 µm, whereas the lower fraction exhibited a surface

205 diameter around 10 µm. The agglomerates sizes of each sample are summarized in Table 1. It
206 should be noted that the sieving process does not modify the size of the agglomerates and
207 only aims at separating the agglomerates according to their sizes. However, the biggest
208 agglomerates, i.e. the less cohesive, may be broken during the sieving process (Deng et al.,
209 2016).

210 *Table 1. Characteristics of the raw and sieved nanocellulose*

Powder	Raw powder	Fine fraction	Large fraction
Sieving size (µm)	N/A	< 40	> 40
Mean surface diameter by sedimentation (µm)	48	10	54
Mean surface diameter 60 ms after dispersion in the 20 L sphere (µm)	10	8	12

211

212 The dust clouds produced after dispersion in the 20 L sphere were also characterized at the
213 moment of ignition, i.e. 60 ms after the dust injection (Table 1). First, it can be confirmed that
214 the injection system tends to break the powder agglomerates, as already shown by previous
215 studies (Du et al., 2015; Sanchirico et al., 2015). Despite the high shear stress induced by the
216 dispersion system of the 20 L sphere, a slight difference in the particle size distributions of the
217 samples can be observed in Figure 3. Indeed, the mean surface diameter obtained by
218 dispersion of the powder sieved below 40 µm is 8 µm whereas the dispersion of the bigger
219 agglomerates (> 40 µm) led to a mean surface diameter of 12 µm. As a comparison, the mean
220 surface diameter by dispersion of the raw powder is 10 µm, which confirms the efficiency of
221 the sieving procedure.

222

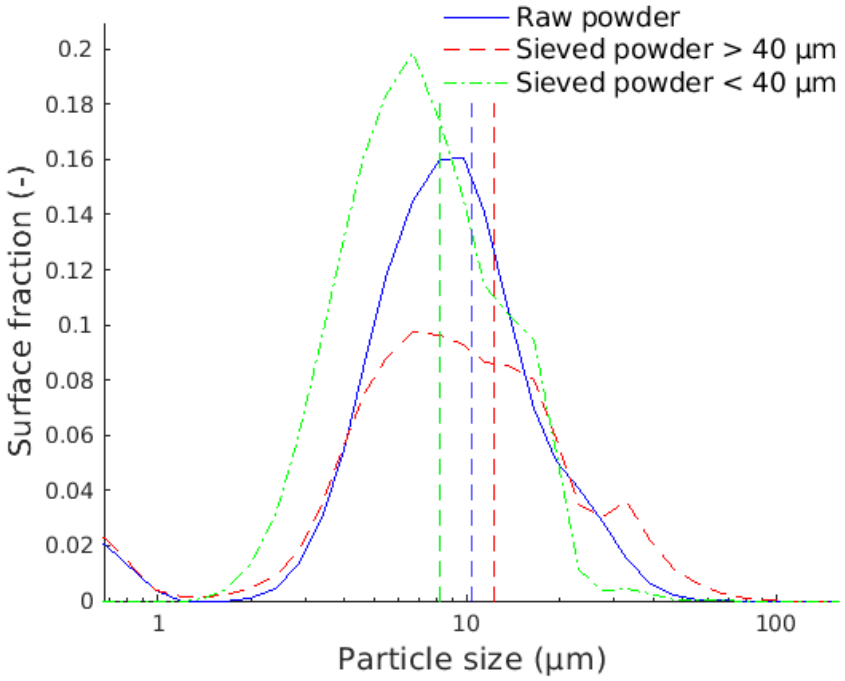

Figure 3. Particle size distribution of raw and sieved nanocellulose after injection in the 20 L at the place and moment of ignition (60 ms after dispersion) measured by the Helos diffraction sensor (R3 lens, 0.5 – 175 µm)

The explosion tests performed on the different samples conduced to rather similar explosion severities, probably due to the small differences in the PSD after dispersion. Indeed, a maximum overpressure of 8.9 ± 0.4 bar and a maximum rate of pressure rise of 555 ± 66 bar.s^{-1} were obtained for the bigger agglomerates (> 40 µm) whereas these values respectively reached 8.7 ± 0.4 bar and 473 ± 56 bar.s^{-1} for the finest powder (Figure 4), which does not constitute a significant difference with regard to the experimental uncertainties. Nevertheless, the lowest concentration inducing an explosion was obtained at 125 g.m^{-3} with the raw powder and the smallest agglomerates and only at 250 g.m^{-3} with the sample of agglomerates bigger than 40 µm. Thus, despite the breakage of the majority of the agglomerates observed in Figure 3, the sample constituted of agglomerates bigger than 40 µm, which contains fewer fine particles than the initial powder, appears to be less ignition sensitive than the two other

samples. This observation tends to corroborate the theory stipulating that the ignition sensitivity of a powder is mainly affected by the presence of fine particles (Saeed et al., 2019) as they are more prone to volatilize.

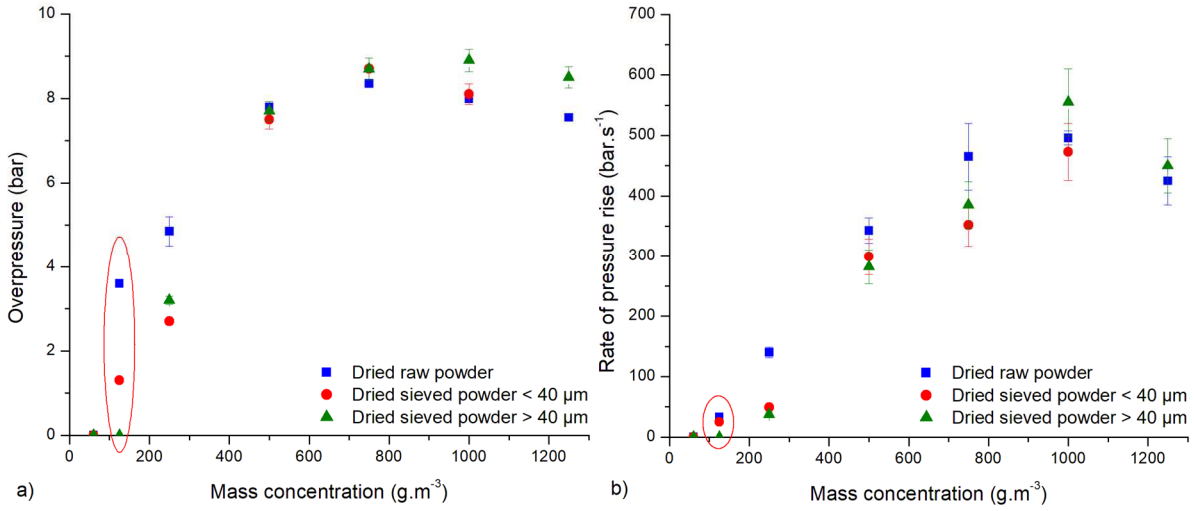

Figure 4. Effects of nanocellulose sieving on a) the maximum overpressure and b) the maximum rate of pressure rise

To further investigate on the influence of fine particles on the ignition sensitivity, ignition energy tests were conducted in the modified Hartmann tube. The minimum ignition energy of the raw dried powder was evaluated at 5 mJ. After drying and sieving at 40 µm, both obtained fractions also presented minimum ignition energies of 5 mJ. As their MIE is lower than 10 mJ, these powders can be considered as being very sensitive to electrostatic ignition (Janès et al., 2008). However, when drying and sieving at 70 µm, the bigger fraction exhibited a minimum ignition energy of 14 mJ. It should be noted that the MIE of microcrystalline cellulose (MCC) ranges from 30 to 100 mJ for 30 µm particles (BGIA, 1997) and previous tests performed on MCC with a mean diameter of 100 µm led to a MIE of 590 mJ .

These tests highlight the effects of the presence of fine particles on the ignition sensitivity, especially for nanomaterials comprised of various sizes of agglomerates. Nevertheless,

sieving is probably not the most accurate method of powder selection, as small particles can stick to agglomerates (due to electrostatic interactions, for instance) and remain in the upper fraction, although smaller than the mesh. Furthermore, for non-spherical particles, only one dimension smaller than the mesh is sufficient for an agglomerate to be retrieved in the low fraction, independently from its volume. As a consequence, in order to stress the influence of agglomeration of nanopowders on their explosion severity and MIE, the impact of mechanical agglomeration has been studied.

3.2. Effects of mechanical agglomeration: example of carbon coated silicon

Since the agglomerates that naturally exist in the raw powder (especially for nanocellulose) are easily breakable and in order to assess the influence of the particle size distribution on the explosion severity, the effects of mechanical agglomeration were investigated through carbon coated silicon (SiΩC). The initial mean surface diameter was measured by sedimentation of the powder using the laser diffraction sensor (Helos – Sympatec) and by wet dispersion in ethanol using a Mastersizer 2000 S (Malvern Instruments). Analyzing the wet dispersion measurements presented in Table 2, it appears that all the agglomerated samples present a mean diameter much higher than that of the raw powder, i.e. 68 µm, and that the powder B exhibits the highest diameter, reaching 442 µm, which is consistent with the SEM observations. However, when regarding the powders agglomerated by process A, it seems that the powder A1 (260 $g.L^{-1}$) is more agglomerated that the powder A2 (400 $g.L^{-1}$), which seems inconsistent with SEM observations. Once again, it should be kept in mind that the wet dispersion in ethanol modifies the interactions between particles (variation of zeta potential) and does not provide accurate information concerning the particle size distribution of a powder in air.

281 The surface diameter was measured by sedimentation of the powder using two lenses of the
282 laser diffraction sensor: R3 and R5 (Table 2). Tests performed with the R3 lens led to rather
283 similar mean surface diameters by sedimentation, from 20 µm to 32 µm, which can be due to
284 the upper limitation of the lens. The R5 lens allows the measurement of particles from 4.5 to
285 875 µm, inducing that the agglomerates observed by SEM can be distinctly observed. First,
286 the powder B is then confirmed to be the most agglomerated ($d_{50,R5}$ = 297 µm), although this
287 was not visible using the R3 lens. Then, the sample A2 presents a lower mean diameter than
288 the sample A1, which is conversely proportional to the particle density and confirms the
289 measurements performed by wet dispersion. Finally, the raw powder presents a mean surface
290 diameter of 207 µm, which is considerably higher than the size of the agglomerates observed
291 by SEM. It should be reminded that this lens does not allow the measurement of particles
292 smaller than 4.5 µm, implying that the small agglomerates may not be measured by the
293 apparatus.

294

295 *Table 2. Mean diameter of the different samples of carbon-coated silicon measured by*
296 *sedimentation and wet and dry dispersion*

	Raw powder	Sample A1	Sample A2	Sample B
Mean diameter by wet dispersion in ethanol (µm) – Mastersizer 2000 S	68	352	261	442
Mean surface diameter by sedimentation – R5 lens (µm) – Helos laser diffraction sensor	207	249	132	297
Mean surface diameter by sedimentation – R3 lens (µm) – Helos diffraction sensor	30	26	32	20
Mean surface diameter after dispersion in the 20 L sphere – R1+R3+R5 Helos diffraction sensor	9	4	3.5	12

Mean surface diameter after dispersion in the Scirocco device (µm) – Mastersizer 2000	3.5	5.3	5	20

297

298 To estimate the PSD during the combustion and specifically at the moment of ignition,
299 dispersion tests were performed with the laser diffraction sensor coupled with the
300 visualization 20 L sphere. Nevertheless, as seen in Table 2, each lens gives a peculiar and
301 useful information on the PSD, but in the case of a nanopowder, a more global view is
302 necessary. Unfortunately, as previously said, no apparatus currently allow such a
303 measurement (from nm to hundreds of micrometers) at high frequency and concentration. An
304 alternative solution could consist in using the same in-situ laser sensor and repeating three
305 times (at least) the same dust dispersion experiment with the three lenses (R1, R3 and R5). In
306 order to normalize the intensities of the peaks, it may be useful to insert an internal reference
307 (nearly monomodal powder of low and fixed concentration, with a narrow PSD which does
308 not interfere with the studied powder). An instance of such application for carbon-coated
309 silicon is given in Figure 5.

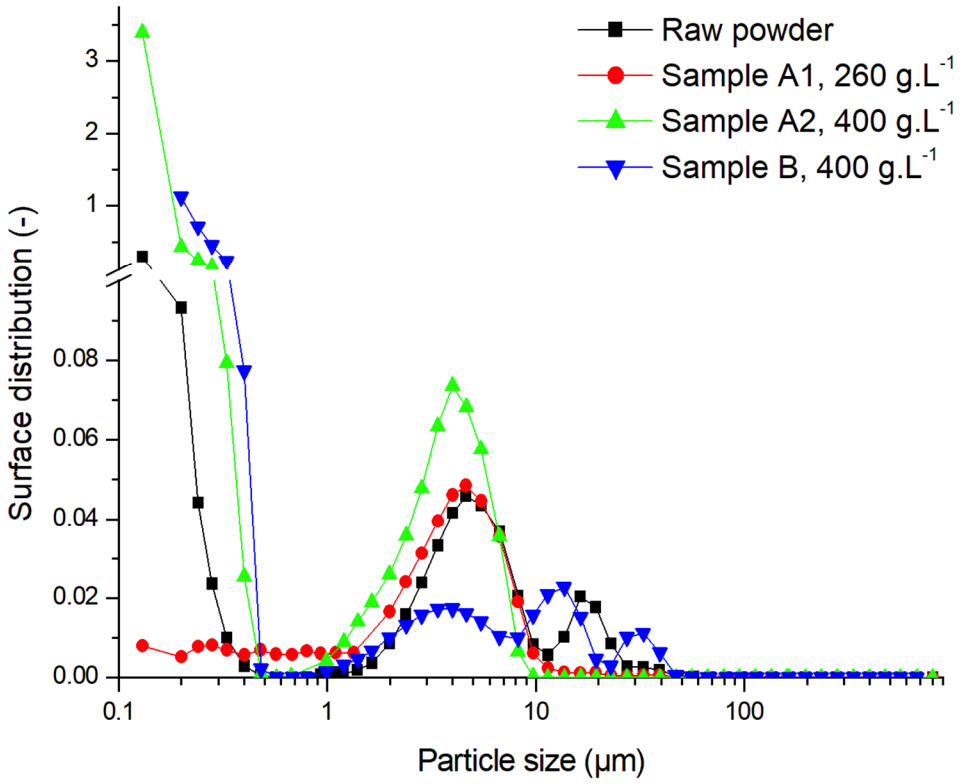

310

311 *Figure 5. Representation of the global PSD of carbon-coated silicon powders after dispersion*
312 *in the 20 L (tv = 60 ms) obtained by the concatenation of PSD measurements done with R1,*
313 *R3 and R5 (Helos – Sympatec)*

314

315 Figure 5 allows the visualization of the PSD of the nanopowders over a wide range of sizes
316 (from 0.1 µm to 875 µm). It appears that sample B (400 $g.L^{-1}$) presents the biggest
317 agglomerates after dispersion in the sphere, with modes at 4, 15 and 35 µm (omitting the
318 primary particles and nanometric agglomerates). The powders A1 and A2 show the smallest
319 agglomerates after dispersion, with mean surface diameters of 4 and 3.5 µm, respectively
320 (Table 2). The raw SiΩC powder, in addition to the common agglomeration mode at
321 approximately 4 µm, also presents larger structures around 20 µm (Figure 5). It should be
322 noticed that, unlike the other samples, no significant peak is obtained for the powder A1 at

particle size lower than 0.5 µm which may seem surprising and requires additional tests with R1 lens.

These observations can lead to several comments: i) The measuring range being limited at 0.1/0.2 µm, the particle size distributions may be different below this value, and the presence of individualized nanoparticles is certainly more marked for the raw powder. ii) The dust injection in the 20 L sphere clearly induces the fragmentation of the biggest structures (Table 2); however, the process B seems to generate more cohesive agglomerates over a wider range of particle sizes. iii) During the agglomeration process, especially with the process A, the structure of the initial agglomerates could have been weakened, reducing the cohesion strength of these initial agglomerates. During particle size measurements by wet dispersion or by sedimentation in air, their structure is not significantly modified. On the contrary, the very high shear rate induced by the dispersion in the 20 L sphere (pressurization at 20 bar) can break these agglomerates, demonstrating the existence of a threshold stress.

Table 2 and Figure 5 demonstrate the fragmentation of agglomerated structures during the injection of SiΩC in the 20 L sphere, but quantitative indicators can be proposed. For instance, a diameter variation, defined by $\Delta D = 100.\frac{(d_{agg}-d_{50})}{d_{agg}}$ was calculated by Sanchirico et al. (2015), who classified the powders into two classes: class 1 containing the hardest dusts ($\Delta D < 50\%$) and class 2 for powders that undergo greater breakage ($\Delta D > 50\%$). By considering only the smaller agglomerates (lens R3), values between 75 % and 98 % were obtained in this work, implying that all the powders are in class 2. It should be underlined that those values are slightly higher than that presented by Sanchirico et al. (2015). Nevertheless, these authors collected the dust several minutes after dust settling, which potentially allows

346 the re-agglomeration of the powder, whereas the measurements in this work were conducted
347 directly within the sphere and correspond to the moment and place of ignition.

348 Dry PSD measurements were also conducted using the Mastersizer 2000 particle size analyzer
349 equipped with a dispersion system called Scirocco (Malvern Instruments). This apparatus
350 allows the measurement of particle sizes from 0.2 to 2000 µm. The powder dispersion is
351 ensured before the measurement by an air jet in a Venturi configuration (Ali et al., 2015;
352 Bonakdar et al., 2016). Although this measurement is not conducted at the same conditions as
353 the explosion tests, the evaluation of the particle size distribution after dispersion of the
354 powder still provides information on the potential agglomerate breakage during the
355 dispersion. The results, also presented in Table 2, are consistent with the SEM images, as the
356 powder B seems the more agglomerated, with a mean surface diameter of 20 µm, whereas the
357 raw powder presents the smallest particles and a mean surface of 3.5 µm. It should be noted
358 that the shear stress induced by the dispersion in the Scirocco device is much lower than that
359 induced during the injection in the 20 L sphere, notably due to a lower dispersion pressure (2
360 barg). Such values tend to show that most of the initial agglomerates are broken during the
361 dispersion in the 20 L sphere, but not necessarily in the Scirocco device, which corroborates
362 that the agglomerates fragmentation depends on the application of a threshold stress.
363 However, a whole characterization of the particle size distribution, from the nanometer to
364 several hundred of micrometers and for both apparatuses, is necessary to conclude on this
365 phenomenon.

366

367 Explosion tests were performed on each sample in the standard 20 L sphere (Figure 6). First,
368 it should be noticed that the increase of overpressure and rate of pressure rise with the dust
369 concentration is very fast, which tends to decrease the accuracy at the 'transition'
370 concentration, i.e. 125 $g.m^{-3}$. Indeed, in this transition zone, a small variation in the dust

concentration can greatly impact the pressure-time evolution. The maximum overpressures obtained are similar independently of the agglomeration state of the sample, reaching around 8.8 bar (Figure 6a), which implies that the same amount of powder seems to react. From the observation of the overpressure evolution with the concentration, agglomeration seems to have a limited effect on the thermodynamic development of the explosion. On the other hand, significant differences appear when regarding the maximum rate of pressure rise obtained for each powder (Figure 6b). The raw powder leads to the most severe explosion, with a maximum rate of pressure of 944 ± 118 bar.s^{-1}. The less agglomerated (at least theoretically) powder i.e. SiΩC A1, is slightly less severe and reaches 822 ± 98 bar.s^{-1}. Both powders are then classified in the St2 class, with explosivity index K_{St} of respectively 256 ± 32 bar.m.s^{-1} and 223 ± 27 bar.m.s^{-1}. The explosions produced by the powders agglomerated with a density of 400 g.L^{-1} are less severe, reaching 713 ± 85 bar.s^{-1} for the sample A2 and only 556 ± 60 bar.s^{-1} for the sample B, which ranks both powders as St1.

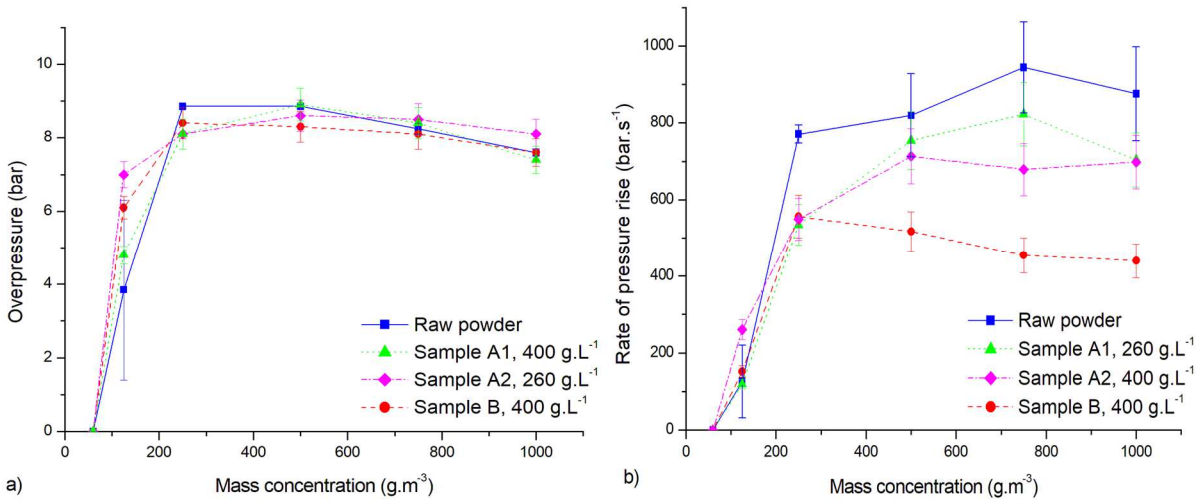

Figure 6. Evolution of the a) maximum overpressure and b) maximum rate of pressure rise as a function of the mass concentration of the four samples of carbon-coated silicon

Then, it appears that only the maximum rate of pressure rise is affected by the agglomeration state of the powder. Considering spherical particles, the density of each powder and the mean surface diameter measured after dispersion in the 20 L sphere (Table 2), the reactive surface area developed after dispersion was calculated for each sample at each concentration. Contrary to the obvious correlations between the explosion severity and the reactive surface observed for starch powders (Santandrea et al., 2019a), no clear relationship could be extracted for the carbon coated silicon. Indeed, if the combustion of organic powder is limited by the pyrolysis step or by the surface reaction of the particles (Di Benedetto et al., 2010), the carbon-coated silicon does not undergo such pyrolysis step. Since the combustion does not occur in gaseous phase, the distance between the particles is of great importance. Indeed, increasing the concentration in the same volume reduces this distance, possibly leading to a transition between the combustion of the individual particle (small concentration) to a group combustion at higher concentrations. On the contrary, promoting the agglomeration tends both to increase the average distance between the combustible structures and to decrease the surface concentration.

After each explosion test, the evolution of the pressure was recorded during the cooling phase. Since the combustion of silicon consumes oxygen and produces silica, the final pressure in the sphere is lower than the atmospheric pressure, even if the combustion of the carbon layer leads to the production of, among others, carbon monoxide and carbon dioxide. The stabilized pressure after explosion can provide information on the combustion gases production and oxygen consumption (Figure 7).

To evaluate the combustion mechanisms, two hypotheses were investigated. First, successive reactions were considered: the carbon C reacts first, followed by the silicon Si (Figure 7). The second hypothesis consists of simultaneous reactions of the carbon and the silicon, the oxygen consumption by each reaction being proportional to the molar proportions of C and Si. The

considered reactions are the formation of carbon dioxide from the carbon and oxygen, and the reaction of silicon with oxygen to form silica (SiO_2). Assuming that the particle diameter is 40 nm with 2 nm of carbon coating, a molar proportion of 27.4% of carbon and 72.6% of silicon was considered. In light of the similar measured overpressures, it was previously established that the reaction products were not significantly affected by the agglomeration state. For a given mass concentration, the same amount of powder is then assumed to be consumed for each sample and the reaction of nitrogen with silicon was neglected.

It appears in Figure 7 that the experimental residual pressure seems to follow the same evolution than in the case of simultaneous reactions of carbon and silicon, even if the carbon layer is the first compound theoretically in contact with oxygen. Such behavior can notably be explained by the combustion of silicon in vapor phase, which is confirmed by considering Glassman's criterion: the boiling point of Si (2355°C) is much lower than the volatilization temperature of its oxide (2950°C for silica) or of its carbon layer (more than 4000°C). As a consequence, after ignition, i.e. at high temperatures, the carbon coating does not prevent or hinder the combustion of the silicon. If the second model seems to represent satisfactorily the experimental data, a concentration shift is visible for the low dust concentrations. Indeed, the value experimentally measured at 125 $g.m^{-3}$ for the raw powder, i.e. around 0.97 bara, corresponds to the value calculated at 60 $g.m^{-3}$ by both models. As a lower pressure would have been theoretically expected, this shift may be due to oxygen adsorbed onto the particles surface, reacting more easily with the carbon layer and generating an extra amount of carbon dioxide. Moreover, Figure 7 shows that the powders agglomerated by the process A, i.e. powders A1 and A2, follows globally the same evolution than the raw powder with a final pressure stabilized around 0.87 bara. On the contrary, the final pressure obtained after combustion of powder B stabilized around 0.89 bara, which confirms the specificity of this powder due to the agglomeration process. Due to the PSD of sample B being greater than

438 those of the other SiΩC powders, the heating rate of such structures is probably slower, which
439 may modify the reaction mechanism, promoting the effect of the carbon layer and thus
440 leading to a lowest explosion severity.

441

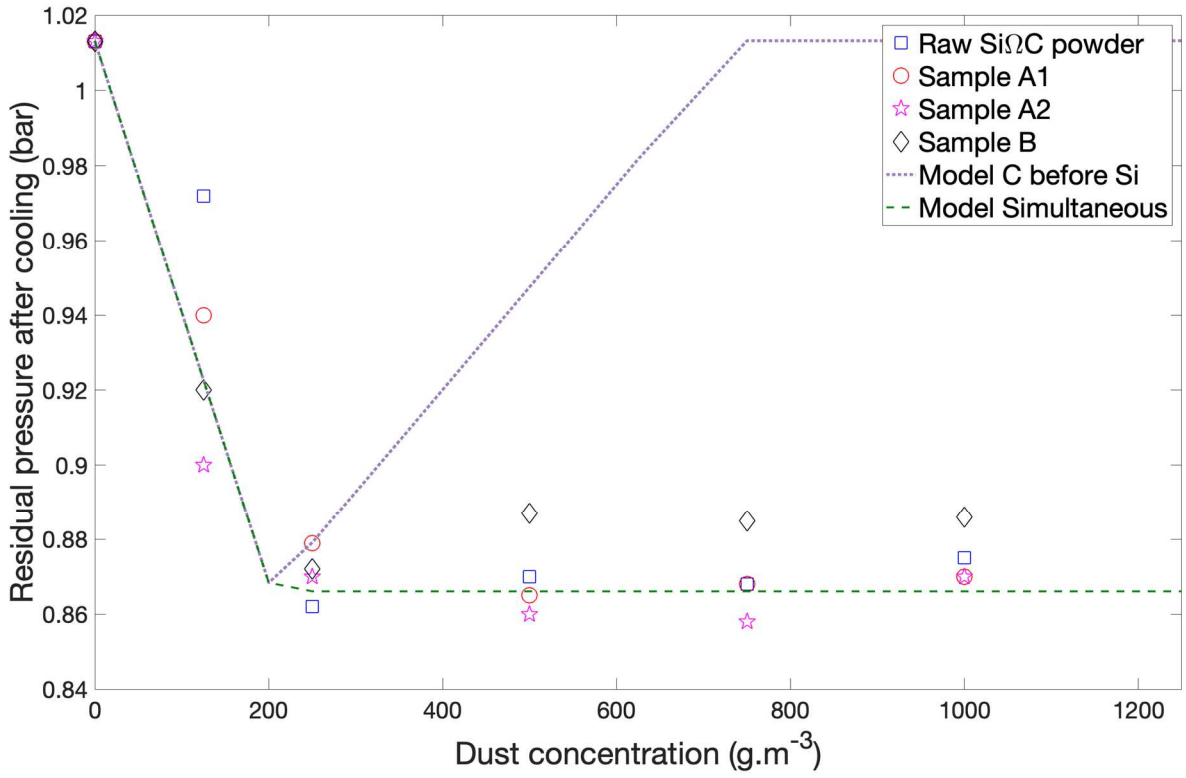

Figure 7. Evolution of the stabilized pressure after explosion in the 20 L sphere with the mass concentration: experimental data for the different samples of carbon-coated silicon and models for the raw powder

In addition to the experiments conducted in the 20 L sphere, the minimum ignition energy (MIE) of the different powders was determined in the modified Hartmann tube according to ISO/IEC 80079-20-2 (2016). While the MIE of the raw powder was evaluated at 5 mJ, no ignition was observed at 1J for the three other samples when varying the dust quantity from 0.6 to 1.8 g and the ignition delay time from 90 ms to 150 ms. Although some glowing particles were observed when testing the sample A1, no flame was obtained. The agglomeration then appears to significantly reduce the ignition sensitivity of SiΩC powders, turning very sensitive raw powders to samples almost insensitive to electrostatic ignition

(Janès et al., 2008). By examining the evolution of the PSD in the tube with the R5 lens, it appears that mean surface diameters of 82 and 252 µm were obtained for raw SiΩC sample and sample B, respectively; which is consistent with MIE results.

Nevertheless, as shown in Figure 6, the lowest concentration for which an explosion was obtained at 10 kJ is the same for all the samples, i.e. 125 $g.m^{-3}$. Since these tests were performed at 10 kJ, additional tests should be conducted with the standard ignition energy to apply to determine the LEL, i.e. 2 kJ (EN 14034-3, 2006). Still, the LEL does not seem significantly modified by the agglomeration state of the powder, which can notably be explained by the strong fragmentation of the agglomerates during the dispersion in the 20 L sphere. Indeed, the agglomerates submitted to the high shear stress of the injection device in the 20 L sphere tend to break more easily than the agglomerates lifted by the air pulse in the modified Hartmann tube, which give them ignition properties similar than the raw powder. This point will be developed in the next section.

3.3. Some theoretical clues on relating the dispersion process and the particle size distribution of nanopowders clouds

Inertia, rotary and turbulent stresses are the three main stresses exerted by the fluid flow on the particles surface. It seems important to consider them as their evolution can explain the deagglomeration phenomenon and thus, the changes in the ignition sensitivity and explosivity previously described.

The inertia stress is due to agglomerates shifts and accelerations in the flow direction. It can be defined by equation 1 (Deng et al., 2016; Weiler et al., 2010):

$$\sigma_I = \frac{\rho}{8}.\left[1 - \frac{\arccos\left(\frac{d_p}{d_{agg}-d_p}\right)}{180°}\right].\left(u_p - u\right)^2.\left[\frac{24}{Re_{rel}} + \frac{24}{Re_{rel}^{0.5}} + 0.4\right] \quad (1)$$

where ρ is the fluid density; d_p, its primary diameter; d_{agg}, the diameter of the agglomerate; u, the flow velocity; u_p, the agglomerate velocity and Re_{rel}, the Reynolds number calculated from the slip velocity u_s between the agglomerates and the gas:

$$u_s = (u_p - u) = d_p^2 \frac{(\rho_p - \rho)}{18.\mu}.a \quad (2)$$

where ρ_p is the particle density; μ the fluid dynamic viscosity and a the acceleration term.

The rotary stress σ_r is generated in zones with high velocity gradient (du/dz). Weiler et al. (2010) defines it as follows:

$$\sigma_r = \frac{\rho_p}{40}.(d_{agg})^2.\left(\frac{du}{dz}\right)^2 \quad (3)$$

Finally, turbulent stresses σ_T caused by the vortices present in the velocity field can also lead to agglomerate breakage both due to impaction between solid structures and to shear stresses. They depend on the ratio between the Kolmogorov scale and the agglomerate size and are expressed as a function of fitting parameters a_i given by Weiler et al. (2010):

$$\sigma_T = a_1 \rho.\left[\frac{\nu_{kin}^{(3a_2-1)}}{l_D^{4.a_2}}\right]^{a_3}.(d_{agg})^{a_4} \quad (4)$$

where ν_{kin} is the kinematic viscosity of the fluid and l_D, the Kolmogorov scale of the flow. The latter parameter can be found for the 20 L sphere at various dispersion times, especially at 10, 50 and 100 ms for Kolmogorov scale (Dahoe et al., 2001; Ogle, 2016). Due to l_D values being unavailable for dust dispersions in the Hartmann tube, they have been evaluated by the following equation:

$$l_D = \left(\frac{\nu_{kin}^3}{\varepsilon}\right)^{0.25} \quad (5)$$

where ε is the turbulence dissipation rate which can be estimated as follows by considering only the vertical direction z:

$$\varepsilon = 15.\nu_{kin}.\left(\frac{du_z}{dz}\right)^2 \quad (6)$$

This assumption made on a privileged direction of the particle flow is confirmed by previous Particle Image Velocimetry (PIV) experiments (Cuervo, 2015). Particles and agglomerates velocities, velocity gradients and acceleration were determined both for the sphere and the tube by CFD simulations and were validated experimentally by PIV measurements (Cuervo, 2015; Murillo, 2016).

Figure 8 shows that the inertia stress is by far the greatest stress which applies on the agglomerates, significantly increasing when d_{agg} increases. The predominance of drag forces on other fragmentation mechanisms is confirmed by other authors (Breuer and Khalifa, 2019) and is illustrated by a Stokes number greater than 90 for a dust dispersion of SiΩC in the sphere, corresponding to large relative velocities between the agglomerates and the flow. However, other mechanisms such as the impaction of large particles on the upper and lower plates of the rebound nozzle (Kalejaiye et al., 2010) should not be neglected. It should be stressed that the calculations were performed for the first 10 ms of the dust dispersion as high acceleration rates specifically occur on short time scales (Murillo, 2016; Weiler et al., 2010).

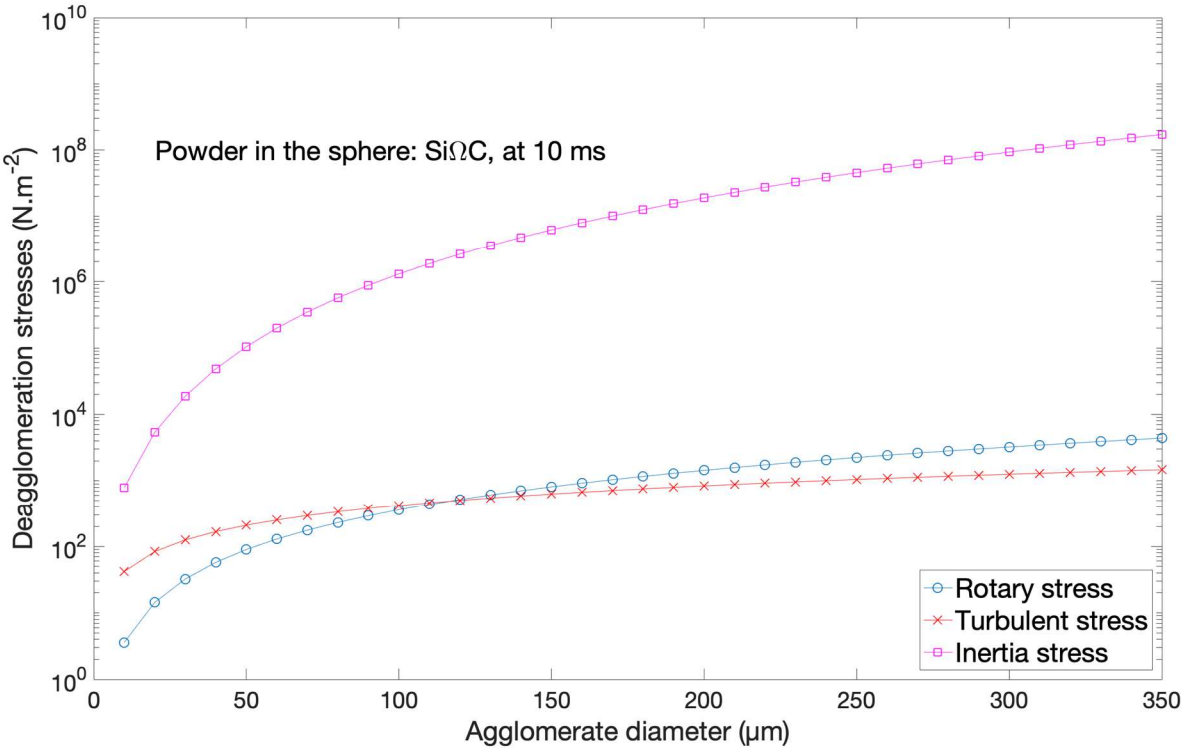

Figure 8. Evaluation of the intensities of the rotary, turbulent and inertia stresses in the 20 L sphere for SiΩC *agglomerates*

Figure 9 represents the evolution of the global stress (sum of inertia, rotary and turbulent stresses) exerted on SiΩC agglomerates both in the 20 L sphere and in the modified Hartmann tube. At first, it can be noticed that, whatever the dispersion time, the stress which applied on the agglomerates in the 20 L sphere is always greater than in the modified Hartmann tube. It can explain why the agglomerated samples of SiΩC showed a minimum ignition energy greater than 1 J as they cannot be fragmented during their dispersion in the tube. On the contrary, Figure 5 demonstrates that the SiΩC samples can be deagglomerated, at least partially, by their injection in the 20 L vessel. As previously said, Figure 9 also confirms that the fragmentation occurs during the first moments of the dust dispersion, when the acceleration and the slip velocity are the greatest. Three models were used to assess the agglomerate strength σ_{agg} and compare it to the deagglomeration stress (Kendall, 1988; Rumpf, 1962; Weiler et al., 2010). Rumpf model assumes that the agglomerate is separated in two parts by a transverse section, without taking into account the actual structure of the agglomerate. It implies that the breakage occurs through a simultaneous rupture of all the bonds along the fracture plan:

$$\sigma_{agg,R} = \frac{9}{8}.\left(\frac{1-\epsilon_p}{\epsilon_p}\right).\frac{F_c}{d_p^2} \quad (7)$$

where ϵ_p is the porosity of the agglomerate and F_c, the cohesion force, limited here to the Van der Waals forces F_{VdW}. With regard to the work presented by Deng et al. (2016), the porosity of SiΩC agglomerates was set at 0.8 and F_{VdW} was estimated through the following relationship valid for 2 identical spheres:

$$|F_{VdW}| = \frac{H.d_p}{24.h_p^2} \quad (8)$$

where H is the Hamaker constant and h_p is the cutoff of separation, set at 0.165 nm (Deng et al., 2016). As Si is coated by a carbon layer, an average Hamaker constant H of $2.5.10^{-19}$ J was chosen, based on the work of Dagastine et al. (2002), indicating that this value is valid for graphite particles in air.

Kendall (1988) claimed that a more gradual rupture occurs and that the real cohesion strength of an agglomerate is overestimated by Rumpf model. As a consequence, the following relation was proposed for the cohesion strength:

$$\sigma_{agg,K} = 15.6\frac{(1-\varepsilon_p)^4}{d_p}.\frac{H}{12.\pi.h_p^2} \quad (9)$$

Finally, Weiler et al. (2010) proposed an alternative model assuming a total breakage of the agglomerates, by considering all the contacts between the particles. Obviously, the cohesion strength of such structure is greater than those obtained by the previous models:

$$\sigma_{agg,W} = \frac{(1-\varepsilon_p)}{\varepsilon_p}.\frac{F_c}{2.d_{agg}^2}.\left[\left(\frac{d_{agg}}{d_p}\right)^3 - \frac{4.\left(1-\frac{Arccos(b)}{180°}\right)}{b^2}\right] \quad (10)$$

with $b = \frac{d_p}{d_{agg}-d_p}$.

In Figure 9, it should be noticed that, even in the 20 L sphere, the stresses are not sufficient to break every Van der Waals bond of SiΩC agglomerates, which is notably confirmed by Figure 5 in which microstructures are still clearly visible. By applying Rumpf model, it seems that only the structures larger than 90 µm will be broken during a dust injection in the 20 L sphere, whereas the limit defined by Kendall model is close to 25 µm. The latter value is consistent with the measurements performed with the laser sensor (Figure 5), but no larger agglomerates are visible after dust dispersion in the sphere, which tends to support Kendall's approach. These conclusions are also in accordance with the Monte Carlo simulations developed by Deng et al. (2016) on 50 nm primary particles. Indeed, they obtained cohesion strengths of $2.8.10^4$ Pa and $1.7.10^5$ Pa for Kendall and Rumpf models, respectively.

Nevertheless, it should be underlined that the cohesion strengths presented in our study should be considered as orders of magnitude as they are greatly dependent on variables which are difficult to quantify, such as Hamaker constant and the cutoff of separation. The same approach can be applied to nanocellulose dispersion, with similar conclusions. However, it will not be detailed here as the fibrous nature of the primary particles makes even more difficult to define their structural properties.

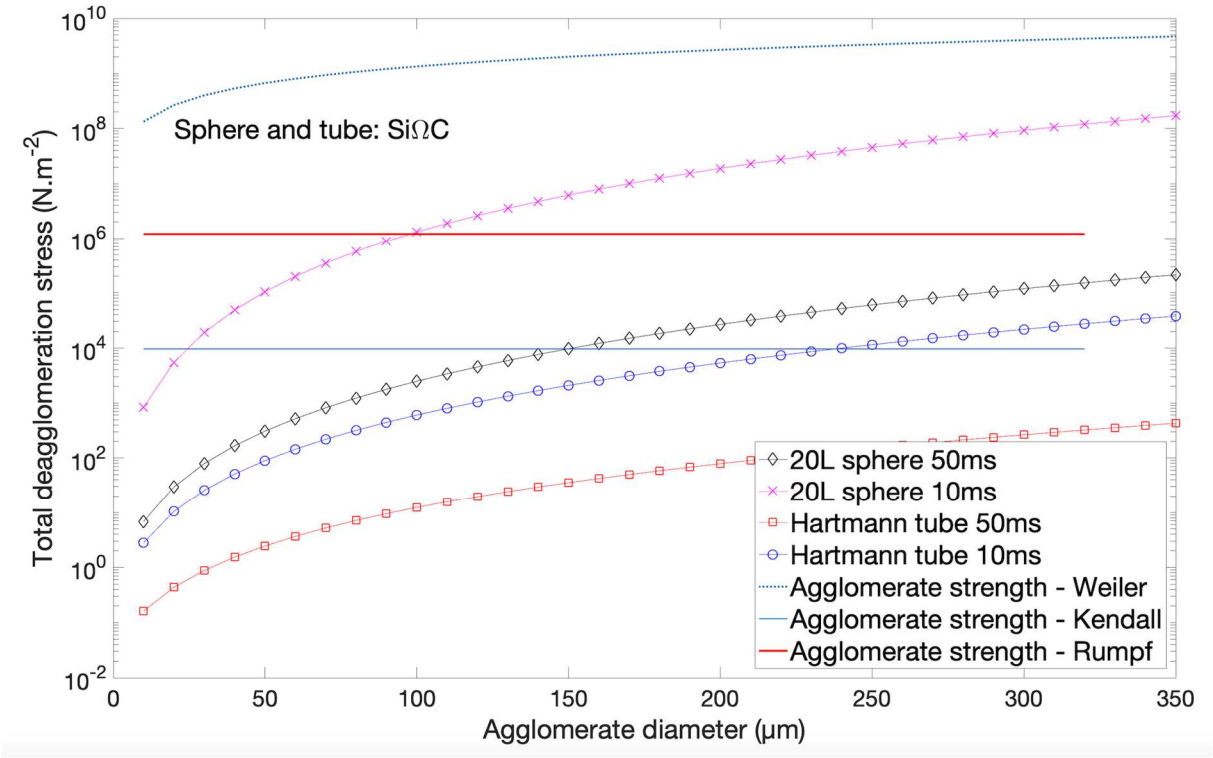

Figure 9. Evaluation of the intensities of the deagglomeration stresses in the 20 L sphere and in the modified Hartmann tube for SiΩC *agglomerates. Comparison with cohesion strengths models.*

4. Conclusions

The ignition and explosion characteristics of nanocellulose and silicon coated by carbon were studied with regard to their agglomeration state, through sieving and mechanical agglomeration. It mainly appears that the agglomerates, naturally or intentionally generated,

578 can be broken if a sufficient stress is applied during their dispersion. The threshold stress can
579 be roughly estimated using models allowing for the determination of the cohesion strength of
580 agglomerates (Kendall model for instance).

581 When applying rather low shear stresses, as for instance during the dust dispersion in a
582 modified Hartmann tube, only the largest structures can be broken, and the minimum ignition
583 energy is greatly modified by the presence of big agglomerates. However, if a greater stress is
584 applied, such as during the dust dispersion in the 20 L sphere, most of the micrometric
585 agglomerates can be broken and the explosion severity is only slightly affected by the
586 presence of brittle agglomerates. But when harder structures are formed, as it is the case for
587 SiΩC produced by the process B, the maximum rate of pressure rise is significantly decreased
588 and the combustion mechanisms can also be altered.

589 Such modification of the explosion risk may be considered as a direct application of the
590 moderation principle of inherent safety. By intentionally agglomerating nanopowders, their
591 ignition sensitivity, but also to a lesser extent, their explosion severity, can be greatly reduced.
592 Nevertheless, it should be underlined that such assertion mainly depends on the stress which
593 will be applied to disperse the powders, during explosion tests, but above all, during an
594 accident. It should be added that a similar approach can be applied to micron-size particles or
595 ultrafine particles.

596 The specificity of the nanopowders lies in their high specific surface area. But a dust cloud of
597 nanopowders (at concentrations greater than the minimum explosive concentration) is always
598 highly polydispersed and the whole particle size distribution has to be considered. Each part
599 of the cloud can ‘play its own role’: the primary nanoparticles influences greatly the ignition
600 step, the primary aggregates or agglomerates of a few micrometers play a significant role in
601 the radiative heat transfer and the bigger micrometric structures can be both considered as

602 flame stretching agents and ‘fuel reserves’. But if the cohesion strength of the agglomerates is
603 too high with regard to the dispersion stress, the explosion risk will be lowered.

604

605 **References**

606 Ali, M., Bonakdar, T., Ghadiri, M., Tinke, A., 2015. Particle Breakage in a Scirocco
607 Disperser. Powder Technol. 285, 138–145.
608 https://doi.org/10.1016/j.powtec.2015.06.048
609 BGIA (1997). Combustion and explosion characteristics of dusts. BIA-Report 13/97 and
610 Gestis Database, HVBG, Sankt Augustin, Germany.
611 Boilard, S.P., Amyotte, P.R., Khan, F.I., Dastidar, A.G., Eckhoff, R.K., 2013. Explosibility of
612 micron- and nano-size titanium powders. J. Loss Prev. Process Ind. 26, 1646–1654.
613 https://doi.org/10.1016/j.jlp.2013.06.003
614 Bonakdar, T., Ali, M., Dogbe, S., Ghadiri, M., Tinke, A., 2016. A method for grindability
615 testing using the Scirocco disperser. Int. J. Pharm. 501, 65–74.
616 https://doi.org/10.1016/j.ijpharm.2016.01.052
617 Bouillard, J., Vignes, A., Dufaud, O., Perrin, L., Thomas, D., 2010. Ignition and explosion
618 risks of nanopowders. J. Haz. Mater. 181, 873–880.
619 https://doi.org/10.1016/j.jhazmat.2010.05.094
620 Breuer, M., Khalifa, A., 2019. Revisiting and improving models for the breakup of compact
621 dry powder agglomerates in turbulent flows within Eulerian–Lagrangian simulations.
622 Powder Technol. 348, 105-125. https://doi.org/10.1016/j.powtec.2019.03.009
623 Cuervo, N. 2015. Influences of turbulence and combustion regimes on explosions of gas- dust
624 hybrid mixture. Université de Lorraine (in English).

625 Dagastine, R.R., Prieve, D.C., White, L.R., 2002. Calculations of van der Waals Forces in 2-
626 Dimensionally Anisotropic Materials and Its Application to Carbon Black. J.
627 Colloid Interface Sci. 249, 78-83.

628 Dahoe, A.E., Cant, R.S., Scarlett, B. On the decay of turbulence in the 20-liter explosion
629 sphere (2001) Flow, Turbul. Combust. 67 (3), 159-184. doi:
630 10.1023/A:1015099110942.

631 Debrincat, D.P., Solnordal, C.B., Van Deventer, J.S.J., 2008. Characterisation of inter-particle
632 forces within agglomerated metallurgical powders. Powder Technol. 182, 388–397.
633 https://doi.org/10.1016/j.powtec.2007.07.001

634 Deng, X., Huang, Z., Wang, W., Davé, R.N., 2016. Investigation of nanoparticle
635 agglomerates properties using Monte Carlo simulations. Adv. Powder Technol. 27,
636 1971–1979. https://doi.org/10.1016/j.apt.2016.06.029

637 Di Benedetto, A., Russo, P., Amyotte, P., Marchand, N., 2010. Modelling the effect of
638 particle size on dust explosions. Chem? Eng. Sci. 65, 772–779.
639 https://doi.org/10.1016/j.ces.2009.09.029

640 Du, B., Huang, W., Liu, L., Zhang, T., Li, H., Ren, Y., Wang, H., 2015. Visualization and
641 analysis of dispersion process of combustible dust in a transparent Siwek 20-L
642 chamber. J. Loss Prev. Process Ind. 33, 213–221.

643 Dufaud, O., Vignes, A., Henry, F., Perrin, L., Bouillard, J., 2011. Ignition and explosion of
644 nanopowders: something new under the dust. J. Phys. Conf. Ser. 304, 012076.
645 https://doi.org/10.1088/1742-6596/304/1/012076

646 Eckhoff, R.K., 2012. Does the dust explosion risk increase when moving from μm-particle
647 powders to powders of nm-particles? J. Loss Prev. Process Ind. 25, 448–459.
648 https://doi.org/10.1016/j.jlp.2011.11.011

649 Eckhoff, R.K., 2011. Are enhanced dust explosion hazards to be foreseen in production,
650 processing and handling of powders consisting of nano-size particles? J. Phys. Conf.
651 Ser. 304(1), 012075. https://doi.org/10.1088/1742-6596/304/1/012075
652 EN 14034-1, 2004. Determination of explosion characteristics of dust clouds — Part 1:
653 Determination of the maximum explosion pressure P_{max} of dust clouds.
654 EN 14034-2, 2006. Determination of explosion characteristics of dust clouds — Part 2:
655 Determination of the maximum rate of explosion pressure rise (dp/dt)max of dust
656 clouds.
657 EN 14034-3, 2006. Determination of explosion characteristics of dust clouds — Part 3:
658 Determination of the lower explosion limit LEL of dust clouds.
659 European Commission, 2011. Recommendation on the definition of a nanomaterial
660 (2011/696/EU). Text with EEA relevance. Official Journal of the European Union
661 Hartley, P.A., Parfitt, G.D., Pollack, L.B., 1985. The role of the van der Waals force in the
662 agglomeration of powders containing submicron particles. Powder Technol. 42, 35–
663 46. https://doi.org/10.1016/0032-5910(85)80036-X
664 Holbrow, P., Wall, M., Sanderson, E., Bennett, D., Rattigan, W., Bettis, R., Gregory, D.,
665 2010. Fire and explosion properties of nanopowders. UK Health and Safety, Executive
666 RR782.
667 ISO/IEC 80079-20-2, 2016. Explosive atmospheres — Part 20-2: Material characteristics —
668 Combustible dusts test methods.
669 Janès, A., Chaineaux, J., Carson, D., Le Lore, P.A., MIKE 3 versus HARTMANN apparatus:
670 Comparison of measured minimum ignition energy (MIE), J. Hazard. Mater. (2008).
671 https://doi.org/10.1016/j.jhazmat.2007.06.066.

672 Kalejaiye, O., Amyotte, P., Pegg, M., Cashdollar, K., 2010. Effectiveness of dust dispersion
673 in the 20-L Siwek chamber. J. Loss Prev. Process Ind. 23, 46-59.
674 https://doi.org/10.1016/j.jlp.2009.05.008

675 Kendall, K., 1988. Agglomerate Strength. Powder Metallurgy 31, 28–31.

676 Krietsch, A., Scheid, M., Schmidt, M., Krause, U., 2015. Explosion behaviour of metallic
677 nano powders. J. Loss Prev. Process Ind. 36, 237–243.
678 https://doi.org/10.1016/j.jlp.2015.03.016

679 Mehta, R.N., Chakraborty, M., Parikh, P.A. Impact of hydrogen generated by splitting water
680 with nano-silicon and nano-aluminum on diesel engine performance (2014) Int. J.
681 Hydrogen Energ., 39 (15), 8098-8105. doi: 10.1016/j.ijhydene.2014.03.149

682 Murillo, C., 2016. Experimental and numerical approaches to particles dispersion in a
683 turbulent flow : application to dust explosions (PhD Thesis). Université de Lorraine,
684 France.

685 Oberdörster, G., Oberdörster, E., Oberdörster, J., 2005. Nanotoxicology: an emerging
686 discipline evolving from studies of ultrafine particles. Environ. Health Perspect. 113,
687 823–839. https://doi.org/10.1289/ehp.7339

688 Ogle, R.A. Dust Explosion Dynamics (2016) Butterworth-Heinemann, 1-639.

689 Rumpf, H., 1962. The strength of granules and agglomerates, Agglomeration. pp. 379–413.

690 Saeed, M.A., Farooq, M., Andrews, G.E., Phylaktou, H.N., Gibbs, B.M., 2019. Ignition
691 sensitivity of different compositional wood pellets and particle size dependence. J.
692 Environ. Manage. 232, 789–795. https://doi.org/10.1016/j.jenvman.2018.11.122

693 Sanchirico, R., Di Sarli, V., Russo, P., Di Benedetto, A. Effect of the nozzle type on the
694 integrity of dust particles in standard explosion tests (2015) Powder Technol., 279, pp.
695 203-208. doi: 10.1016/j.powtec.2015.04.003

696 Santandrea, A., Bonamis, F., Pacault, S., Vignes, A., Perrin, L., Dufaud, O., 2019a. Influence
697 of the Particle Size Distribution on Dust Explosion: How to Choose the Right
698 Metrics? Chem. Eng. Trans. 77, 667–672. https://doi.org/10.3303/CET1977112
699 Santandrea, A., Pacault, S., Perrin, L., Vignes, A., Dufaud, O., 2019b. Nanopowders
700 explosion: Influence of the dispersion characteristics. J. Loss Prev. Process Ind.
701 https://doi.org/10.1016/j.jlp.2019.103942
702 Santandrea, A., Vignes, A., Krietsch, A., Brunello, D., Perrin, L., Laurent, A., Dufaud, O.,
703 2020. Evaluating the explosion severity of nanopowders: international standards
704 versus reality. Process Saf. Environ. Prot. 138, 279-
705 291.https://doi.org/10.1016/j.psep.2019.12.018
706 Sokolov, S.V., Tschulik, K., Batchelor-McAuley, C., Jurkschat, K., Compton, R.G., 2015.
707 Reversible or not? Distinguishing agglomeration and aggregation at the nanoscale.
708 Anal. Chem. 87, 10033–10039. https://doi.org/10.1021/acs.analchem.5b02639
709 Stark, W.J., Stoessel, P.R., Wohlleben, W., Hafner, A., 2015. Industrial applications of
710 nanoparticles. Chem. Soc. Rev. 44, 5793–5805. https://doi.org/10.1039/C4CS00362D
711 Walter, D., 2013. Primary Particles - Agglomerates - Aggregates, in: Deutsche
712 Forschungsgemeinschaft DFG (Ed.), Nanomaterials. Wiley-VCH Verlag GmbH &
713 Co. KGaA, Weinheim, Germany, pp. 9–24.
714 https://doi.org/10.1002/9783527673919.ch1
715 Weiler, C., Wolkenhauer, M., Trunk, M., Langguth, P., 2010. New model describing the total
716 dispersion of dry powder agglomerates. Powder Technol. 203, 248–253.
717 https://doi.org/10.1016/j.powtec.2010.05.015
718 Wu, H.-C., Chang, R.-C., Hsiao, H.-C., 2009. Research of minimum ignition energy for nano
719 Titanium powder and nano Iron powder. J. Loss Prev. Process Ind. 22, 21–24.
720 https://doi.org/10.1016/j.jlp.2008.10.002

721 Wu, H.,C., Wu, C.W., Ko, Y.H. (2014). Flame phenomena in nanogrinding process for
722 titanium and iron, J. Loss Prev. Process Ind. 27, 114-118.
723 http://dx.doi.org/10.1016/j.jlp.2013.11.002

724